

Exciton-induced lattice relaxation and the electronic and vibrational spectra of silicon clusters

Jakyoung Song

*Department of Physics and Astronomy and Condensed Matter and Surface Sciences Program,
Ohio University, Athens, Ohio 45701-2979*

Sergio E. Ulloa

*Department of Physics and Astronomy and Condensed Matter and Surface Science Program,
Ohio University, Athens, Ohio 45701-2979
and Sektion Physik, Ludwig-Maximilians-Universität München, Gesch.-Scholl-Platz 1, D-80539 München, Germany*

David A. Drabold

*Department of Physics and Astronomy and Condensed Matter and Surface Sciences Program, Ohio University, Athens, Ohio 45701-2979
(Received 15 September 1995)*

The geometrical structures and electronic and vibrational spectra of silicon clusters with 20, 60, and 70 atoms are investigated. Using a first-principles quantum-molecular-dynamics method we obtain the equilibrium structures, and study the effects of an exciton-induced lattice relaxation in these systems. The relaxation induced by the exciton may result in a strong distortion of metastable structures, accompanied by changes in the electronic and vibrational spectra. This photoinduced deformation is associated with the presence of nearly degenerate electronic states in the metastable structure, similar to spontaneous Jahn-Teller distortions. The distortion yields lower symmetry and energy, suggesting the trapping of excitons in some of these structures.

I. INTRODUCTION

The competition between geometrically symmetric features that distribute strains evenly and the requirements for appropriate bonding characteristics (angles, bond lengths, etc.) determine the equilibrium structure of small covalent clusters. The particular case of silicon clusters is illustrative of this competition, and has received a great deal of attention in recent years both from experimental and theoretical groups.¹⁻²² While a high degree of stability is achieved in small to medium size *carbon* clusters by a variety of highly symmetric fullerene structures,²³ such is not the case in silicon. The tendency of the latter to preferentially form sp^3 bonds appears to inhibit the formation of many symmetric fullerene-like structures. To what degree this fourfold bonding environment has to be satisfied while introducing strains due to finite-size and/or surface effects has been the subject of some debate in the literature.¹⁻²²

On the experimental side, a number of interesting observations in small silicon clusters have been reported.⁶⁻¹⁰ Although no “magic numbers” in intermediate-size silicon clusters have been identified with regard to the stability or abundance of clusters, it has been found that clusters with 25, 33, 39, and 45 silicon atoms exhibit lower chemical reactivity.⁷⁻⁹ At the same time, the optical spectra of neutral clusters with 18 to 41 silicon atoms show that all these clusters have essentially identical photodissociation energy.¹⁰ Moreover, although detailed structural studies of small clusters are not possible experimentally, cluster diffusion experiments suggest an interesting transition from prolate to spherical or oblate shape for clusters with more than 27 atoms.³

The equilibrium structures and bonding in small silicon clusters have been investigated theoretically using several

approaches.^{1,2,4,5,11,22} A combined tight-binding and density-functional-theory scheme was used to calculate the structural stability and electronic properties of silicon clusters up to 14 atoms.¹ The electronic and vibrational spectra of equilibrium structures of small clusters have also been obtained using a first-principles electronic method based on the Harris functional version of the local density approximation.² These results were in excellent agreement with experiment and other first-principles calculations for small Si clusters.

For larger silicon clusters, fullerenes and possible “magic number” cluster stability have been studied theoretically also by several techniques.¹²⁻²¹ An approximate tight-binding molecular-dynamics approach was used to examine the structure of various clusters, including 50, 60, and 70 atoms.¹² Moreover, the equilibrium geometry of Si_{60} has been studied by a semiempirical method¹³ and a generalized tight-binding molecular-dynamics scheme.¹⁴ According to Menon and Subbaswamy, a compact network structure of Si_{60} obtained after relaxation of the cluster built from blocks of bulk diamond structure is more stable than the C_{2h} symmetry fullerene-like structure of Si_{60} . Other interesting structures, such as cylindrically stacked benzenelike or naphthalenelike structures, have also been used to explain the fragmentation spectra of Si_6 and Si_{10} ,⁶ and compared with fullerene-like cage structures.^{15,16} The latter structures are found to be more stable than the stacked geometries.¹⁶

In a related development, Röthlisberger, Andreoni, and Parrinello found that the structure of silicon clusters consists of two shells of atoms in Si_{45} .¹⁸ Here, the outer shell has the shape of a fullerene-like cage with either 38 or 39 atoms, while the inner core atoms show high coordination as they saturate dangling bonds introduced by the finite size. Recently, Menon and Subbaswamy have presented a thorough stability analysis of various models proposed for the Si_{45}

cluster,^{16,18,19} using their generalized tight-binding molecular-dynamics approach.^{20,21} They find that it is indeed the lower symmetry clusters that have the lowest energy and exhibit a highly coordinated core, just as proposed in Ref. 18. At least for this size, the geometry of the cluster forces overcoordination in the core atoms.

In this context, we present here a detailed study of a small cluster, Si_{20} , and intermediate size clusters, Si_{60} and Si_{70} . The latter have fullerene-like metastable structures with slightly higher energy than the compact network lowest-energy structures, while Si_{20} , consisting of just 12 pentagons, does not have a fullerene-like metastable structure with threefold coordination. This difference would point perhaps to the additional stability of the geometry in the fullerene structure. We find that the minimum configurations are all of the compact network (high coordination) type. The network structures in Si_{60} and Si_{70} have a more spherical shape than Si_{20} , showing a similar structural transition to that suggested by Ref. 3 for Si_n^+ ions. The lowest-energy structures are found to be closely packed clusters with an overcoordinated core. We study their structural properties, as well as the electronic level structure and vibrational spectra, and explore the stability of the fullerene structures under thermal excitations. Incidentally, we find that the binding energy per atom in all clusters studied is very similar (in the network configurations), in agreement with the lack of magic numbers described above.

Moreover, we study the stability of the structures under exciton-induced lattice relaxations, which could be explored in photochemistry experiments. We find that, similar to the case of partly ionic compounds,²⁴ a self-trapping of the exciton occurs whenever the induced lattice distortion splits the nearly degenerate states of metastable clusters, lowering the symmetry of the structure and the overall energy of the system. This effect is reminiscent of the Jahn-Teller effect in neutral and charged carbon clusters, as discussed recently by Adams *et al.*,²⁵ the self-trapping of core excitons and valence biexcitons in bulk diamond, as discussed recently by Mauri and Car,²⁶ and the effects of light-induced network reorganization in *a*-Si (the Staebler-Wronski effect), as studied by Fedders, Fu, and Drabold.²⁷

In photochemistry, the light-induced distortion is an example of an “internal conversion” which allows for physical relaxation of the structure before a perhaps radiative decay or recombination of electron-hole pair.²⁸ Notice also that this “photosensitivity” can be used to explore the stability of various structures, as the absorption coefficient of an assembly of clusters would change dramatically under light exposure.

The remainder of the paper is organized as follows. We briefly outline our theoretical approach in Sec. II. Here, we introduce the first-principles molecular-dynamics technique of Sankey and co-workers.²⁹ We also describe the simulation processes to obtain the equilibrium structures, the vibrational spectra, and exciton-induced lattice relaxation. In Sec. III, we discuss the resulting geometrical structures and the electronic and vibrational spectra of the equilibrated fullerene-like structures for silicon clusters of 20, 60, and 70 atoms. Finally, in Sec. IV, we present a brief discussion and conclusions.

II. THEORETICAL APPROACH

(a) *Molecular dynamics.* The first-principles quantum molecular-dynamics method developed by Sankey and co-workers is used in this paper.²⁹ This method is based on the density-functional theory (DFT) within a pseudopotential scheme, and makes a number of approximations that simplify the electronic structure calculation to give efficient and accurate results in good agreement with experimental and other theoretical data.^{1,2} A complete description of the main approximations used^{30–33} is presented by Sankey *et al.*^{2,29}

This local basis LDA method has been tested for the electronic and vibrational spectra and equilibrium structures of small silicon clusters of up to seven atoms.² The results are in good agreement with experiment,³⁴ and other first-principles methods for small silicon clusters.¹ The method yields acceptable accuracy with moderate execution time in the investigation of various covalent systems. It has also proven very useful in the description of various bulk systems, surfaces, and amorphous materials.³⁵ Notice that although this technique is more computationally intensive than semiempirical approaches, its transferability is amply demonstrated,³⁵ and it does not involve fitting to experimental data. It is *ideal* for clusters, where the periodicity imposed by selecting a plane-wave basis is highly inappropriate.

(b) *Initial geometry equilibration.* We start our analysis considering ideal structures: spheroidal hollow ideal fullerenes with the highest symmetry obtained from the corresponding carbon structures after proper scaling to Si-Si bond lengths, which represent the minimum energy ideal structure for each case studied. The metastable and equilibrium structures that follow are obtained by employing both annealing and quenching processes.²⁹ In the *annealing* method, we subject the cluster to large temperatures and relax the system for enough time (typically 4800 fs) to achieve a highly disordered structure. We use various annealing temperatures to explore the stability of the equilibrated structures, typically a few thousand degrees Kelvin. After annealing for enough time, the structure is “cooled” using the *dynamical quenching* technique. In the dynamical quenching process, the temperature of the structure is reduced by removing the kinetic energy of the atoms (setting the individual velocities to zero) every time the global kinetic energy reaches a maximum during the molecular-dynamics runs. The repeated removal of the excess kinetic energy drives the system into a continuously lower-energy state, finally leaving it in a metastable (and likely the lowest-energy or “equilibrium”) configuration. The lowest-energy structures are obtained when the high-temperature annealing and the successively lower (room) temperature annealing are performed before the quenching, while metastable structures are obtained when just a dynamical quenching run is performed starting from the ideal fullerene cluster geometries.

In the small- and intermediate-size ranges, we study clusters with 20, 60, and 70 atoms. Each cluster size is configured initially in the ideal fullerene cage structure with an overall scaling having the minimum energy in each case, and then either quenched only or quenched and annealed, in order to equilibrate the system. The resulting structures are then compared (after repeated annealing and quenching, in one case, to ensure that we find the lowest-energy state) as

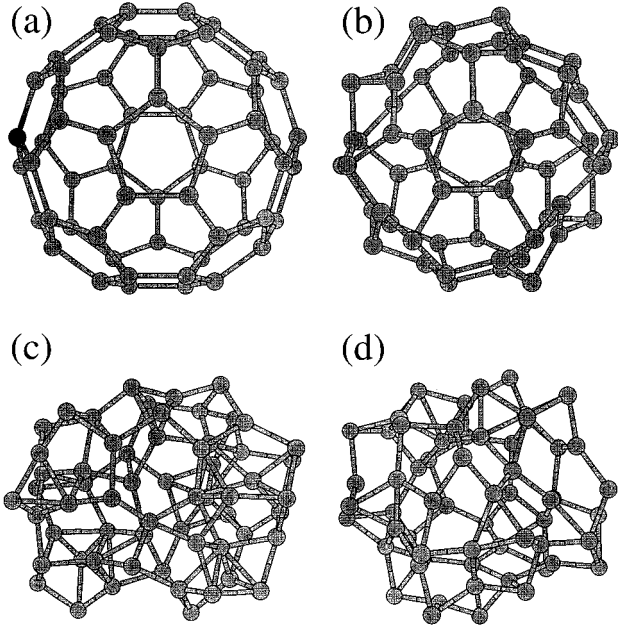


FIG. 1. Si_{60} cluster: (a) The initial ideal configuration of the silicon fullerene structure. (b) Metastable fullerene-like cage structure after just quenching of (a) is performed. (c) Equilibrium network structure after repeated annealing and quenching are performed. This is the lowest-energy cluster found. (d) Metastable fullerene-like cage structure with exciton after lattice relaxation. Notice strong reconstruction associated with exciton self-trapping.

far as the total energy per atom, pair-correlation functions, electronic state spectrum, and the harmonic vibrational spectrum, as described below.

(c) *Vibrational modes.* The vibrational spectra for each equilibrium and metastable structure are obtained by constructing and diagonalizing the dynamical matrix of the structure, $\phi_{\alpha\beta}^{ij}$. This is obtained by displacing atom i from its equilibrium position by a small distance δr in the α direction, and calculating the forces acting on atom j in the direction β . Here, $\alpha = x, y, z$ and $i = 1 - N$, where N is the total number of atoms. The calculated matrix and properties are insensitive to the value of δr for $0.01 \leq \delta r \leq 0.05 \text{ \AA}$. The diagonalization of the dynamical matrix yields the harmonic mode frequencies of the system, together with their eigenvectors, which can be analyzed to gain physical insights into the nature of the various modes.

(d) *Valence excitons.* In order to study the stability of the clusters under photoexcitations, we “create” a valence exciton by promoting an electron from the highest valence-band state to the lowest conduction-band state [a highest occupied molecular orbital (HOMO) to lowest unoccupied molecular orbital (LUMO) change of occupation numbers]. We then allow the structure with this excitation to undergo lattice relaxation, but keeping the *electronic* level occupation in an excited configuration. This approach for the estimation of *excited* states of the structure is not in violation of the variational principle used in DFT for the *ground-state* configuration. Moreover, this approach has been used with excellent results in the study of $1s$ core excitons in diamond,^{26,36} surface bipolarons in GaAs,²⁴ and light-induced defects in $\alpha\text{-Si}$,²⁷ for example. Notice that this approach ignores pos-

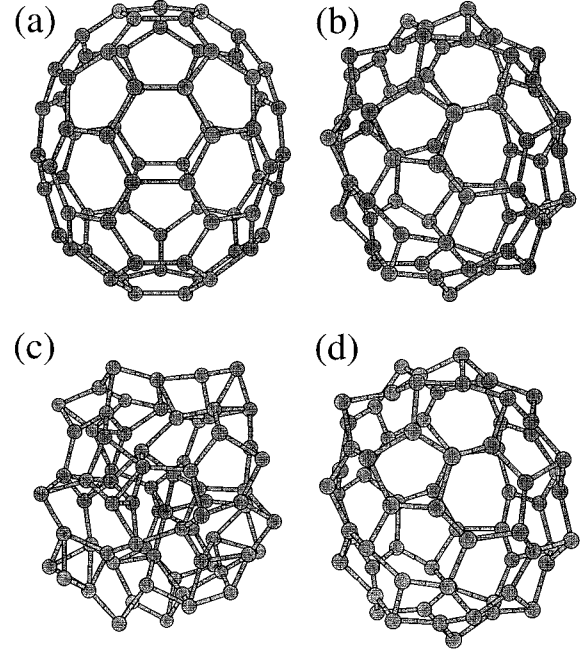


FIG. 2. Same as Fig. 1, but for the Si_{70} cluster (a) to (d): (a) Ideal fullerene configuration. (b) Metastable cage after just quenching of (a). (c) Lowest-energy configuration achieved after repeated annealing and quenching processes. (d) Metastable fullerene-like cage structure with exciton after lattice relaxation. Almost no change with respect to (b).

sible quasiparticle self-energy corrections, but these are expected to be small in comparison with the energy changes we report below.³⁷

III. RESULTS

A. Geometrical structures

In Figs. 1, 2, and 3, the characteristic geometry of the various structures is shown for different relaxation configurations. Figures 1(a), 2(a), and 3(a) show the ideal fullerene-like cage for Si_{60} , Si_{70} , and Si_{20} , respectively. These structures were obtained from the corresponding carbon fullerene structures after rescaling the bond lengths from bulk C-C (1.54 \AA) to bulk Si-Si values (2.43, 2.44, and 2.45 \AA for Si_{60} , Si_{70} , and Si_{20} , respectively; notice that these numbers are chosen so as to obtain the minimum energy of the ideal structure). These structures have an obviously high degree of symmetry while being strongly unstable, since the necessary sp^2 bonding is not energetically favorable in silicon.

After dynamically quenching (no annealing) the ideal Si fullerenes, they relax into a structure as those shown in Figs. 1(b) and 2(b), respectively. Notice that the overall coordination of the atoms in the cluster is not changed, but the geometry is now strongly distorted, with buckled surface hexagons and pentagons, as one or another of the member of each face is pushed either outward or inwards into the shell. One of the main reasons for the different geometrical structures between Si and C clusters appears to be the different covalent radius (that of silicon, 1.11 \AA , is much larger than in carbon, 0.77 \AA) and the corresponding tendency of Si to form sp^3 bonds. However, the quenched structures show a

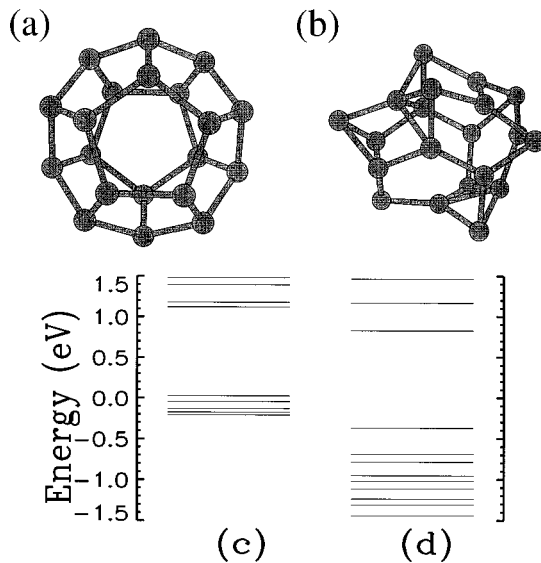


FIG. 3. Si_{20} cluster: (a) Ideal fullerene configuration. (b) Equilibrium network structure after repeated annealing and quenching processes. (c) and (d) are electronic energy levels near the Fermi level for different geometries of Si_{20} , corresponding to (a) and (b), respectively.

high degree of stability, resisting further distortion after annealing at moderate temperatures (a few hundred degrees Kelvin). Notice further that the quenched Si_{60} structure in Fig. 1(b) has only 0.23 eV/atom higher energy than the fully annealed (equilibrium) structure in Fig. 1(c). The corresponding value for Si_{70} is 0.24 eV/atom.

In contrast with the robust stability of the quenched clusters above, the Si_{20} cluster does *not* have a fullerene-like *metastable* structure with threefold coordination, even though the structure is relaxed from the ideal symmetrical structure. The initial structure of Si_{20} consists of just 12 pentagons, as shown by Fig. 3(a). This difference would point to the additional stability of the geometry in the fullerene structure. Perhaps it would be interesting to see whether the *metastable* structures have a preference for different geometries (fullerene or not), as we find below that the equilibrium (ground-state) configurations are all of the network type, as shown in Figs. 1(c), 2(c), and 3(b). If this were the case, one would in principle expect to have a somewhat larger abundance of the fullerene clusters if the creation process were carried out at relatively low energy and/or temperature and no annealing of all the structures occurred immediately after production.

Moreover, we explore a 20-atom (C_{3v}) elongated structure proposed in Ref. 22 in order to compare to the ideal fullerene cage (dodecahedron) structure. The elongated structure is found to have 0.3 eV/atom lower energy than the latter case, in agreement with Grossman and Mitas.²² However, the quenched structure obtained from the elongated structure shows a compact network type, very close to the annealing result of the ideal fullerene geometry, except for having 0.16 eV/atom higher energy than the fully annealed structure. These comparisons lead to the conclusion that both shell geometries of Si_{20} allow for high coordinations after relaxation (even if only quenching is performed) unlike the

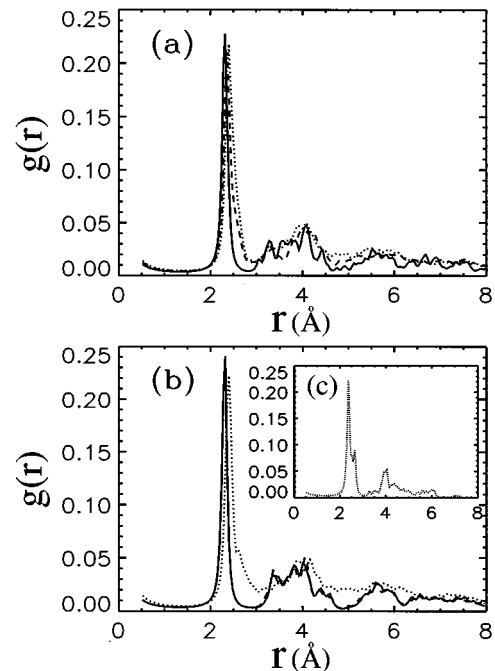


FIG. 4. Radial distribution function. (a) Si_{60} , (b) Si_{70} . Solid line is for fullerene-like metastable structure; dotted line is for network equilibrium structure; dashed line is for fullerene-like structure with exciton. Inset: (c) Si_{20} for network equilibrium structure.

relaxation results of Si_{60} and Si_{70} . This difference would result from the fact that the diameter of the shells in Si_{20} is not large enough to avoid bonding to the neighbor between sides, while the diameters in Si_{60} and Si_{70} appear to be. Full annealing of the elongated structure has a similar minimum energy to the one obtained from the fullerene structure [Fig. 3(b)]. However, the structure shows higher average coordination and a slightly more prolate shape than the latter case.

Figures 1(c) and 2(c) show the equilibrium network structures obtained after annealing and quenching are performed in the ideal fullerenes. All the structures obtained in repeated annealing and quenching runs have similar coordination and geometrical arrangements as those shown in Figs. 1(c) and 2(c) (the cluster shown is the one found with the lowest energy). Similarly to the structures reported by Röthlisberger, Andreoni, and Parrinello for Si_{45} clusters,¹⁸ the equilibrium structures we find are not hollow shells, containing a small inner core cluster with a high degree of coordination. The higher coordination appears to also stabilize here the dangling bonds introduced by the surface curvature. By measuring the diameter of the network structures in Figs. 1(c), 2(c), and 3(b), we obtain that the network structures in Si_{60} and Si_{70} are slightly more oblate in shape than Si_{20} (with minor to major axis ratios of 1.23, 1.33, and 1.47, respectively). This behavior for the neutral clusters is in general agreement with experiments suggesting a structural transition in charged Si_n^+ clusters.³

Additional structural information can be obtained by calculating the radial distribution function of each structure, as shown in Fig. 4. Figure 4(a) shows the results for the Si_{60} cluster, and 4(b) for Si_{70} . The solid lines show results for the metastable structures in Figs. 1(b) and 2(b), respectively. Notice the sharp nearest-neighbor peak at ≈ 2.32 Å, followed by

TABLE I. Total structural energies (relative values with respect to lowest-energy structure in parentheses), and energy gap between LUMO and HOMO, E_g (eV), for Si_{20} , Si_{60} , and Si_{70} clusters.

| Size | Geometry | Stability | Energy/atom (eV) | E_g (eV) |
|------|----------------------|--------------------------------------|------------------|------------|
| 20 | Ideal fullerene-like | Unrelaxed | -106.70(+0.46) | 0.07 |
| | Network | Annealing+quenching | -107.16(0.0) | 1.20 |
| 60 | Ideal fullerene-like | Unrelaxed | -107.00(+0.31) | 0.98 |
| | Fullerene-like | Metastable (just quenching) | -107.08(+0.23) | 0.94 |
| | Network | Equilibrium (annealing+quenching) | -107.31(0.0) | 0.74 |
| | Metastable+exciton | Metastable | -107.20(+0.11) | 0.06 |
| 70 | Ideal fullerene-like | Unrelaxed | -107.00(+0.33) | 0.97 |
| | Fullerene-like | Metastable (just quenching) | -107.09(+0.24) | 0.56 |
| | Network | Equilibrium (annealing+quenching) | -107.33(0.0) | 0.73 |
| | Metastable+exciton | Metastable | -107.08(+0.25) | 0.29 |

a relatively broad distribution of next-nearest-neighbor bond lengths between 3 and 4.2 Å, for both the 60 and 70 clusters. After full equilibration and/or relaxation, corresponding to the structures in Fig. 1(c) and 2(c), the pair distribution function is shown by the dotted lines in Figs. 4(a) and 4(b). The most noticeable effect of the relaxation is to broaden the nearest-neighbor bond lengths rather dramatically, in addition to a small lengthening of the bonds (to ≈ 2.40 Å), as shown by the shifted main peak. The equilibrated structure is clearly less symmetric, as the overall background of possible bond lengths increases, yielding a nearly uniform $g(r)$ for larger r values, as one would expect in a fully homogeneous configuration. Figure 4(c) shows the pair distribution function for Si_{20} , corresponding to the fully relaxed structure in Fig. 3(b). The sharp nearest-neighbor peak is at ≈ 2.36 Å while the bond lengths at the small peak near 2.6 Å are due to the rearrangement between two atoms with threefold bonds, leading to fourfold bonds in the relaxed structure. A smaller but sharp feature near 4 Å indicates a homogeneous distribution of second nearest neighbors in this small structure.

Table I summarizes the total energies of the Si_{20} , Si_{60} ,

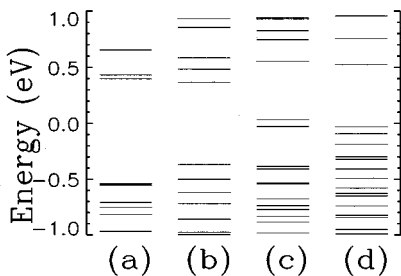


FIG. 5. Electronic energy levels near the Fermi level for different geometries of Si_{60} . (a) Fullerene-like metastable cage structure; (b) network (lowest-energy) structure; (c) fullerene-like cage structure after exciton induced (with lattice relaxation); and (d) system with exciton is again lattice relaxed after exciton removal.

and Si_{70} clusters. Also shown are the HOMO-LUMO gaps (see below). We have also calculated the binding energy per atoms for the ideal structure in Si_{20} . The results show good agreement with Kaxiras and Jackson.¹⁷ The binding energy per atom for the ideal structures in Si_{60} and Si_{70} also follows the general behavior for spherical clusters discussed in Ref. 17.

B. Electronic spectra

The strong reconstructions observed after quenching and annealing are of course accompanied by a change in the overall electronic energy spectra of the clusters. The resulting energy levels near the Fermi energy are shown in Figs. 5 and 6 for Si_{60} and Si_{70} , respectively. The Fermi energy is shown as zero here. Set of levels (a) and (b) correspond to the fullerene-like metastable cage, and the fully relaxed network structure, respectively. In both the 60 and 70 cluster cases, the full relaxation is particularly accompanied by a breaking of degeneracies in the various levels near the Fermi energy. However, in the case of Si_{60} , the gap between the highest filled orbital and the lowest empty one (the “HOMO-LUMO gap”) decreases after the full relaxation, while in Si_{70} it increases. In the 60 cluster, this gap (denoted by E_g in Table I) changes from 0.94 eV in the metastable structure to

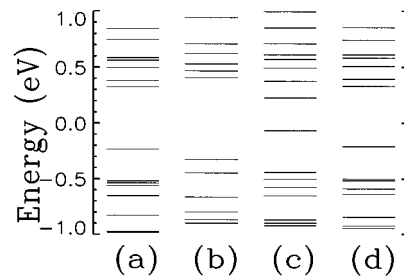


FIG. 6. Same as Fig. 5 but for Si_{70} .

0.74 eV in the fully relaxed network cluster. In contrast, the gap changes from 0.56 to 0.73 eV for the Si_{70} cluster. (Notice that although our calculations are likely to overestimate the HOMO-LUMO gap because of the finite-size basis used, the comparison between structures is real, reflecting the different dynamics and structural rearrangements for each structure.)

Because of the high symmetry of the ideal fullerene cage, some of which remains in the buckled metastable structures of Figs. 1(b) and 2(b), the corresponding electronic structure exhibits degeneracy or near degeneracy of a number of occupied orbitals. This degeneracy is, however, split by the distortions of the cluster under quenching, by a mechanism akin to the Jahn-Teller effect in various solids, as discussed recently by Khan and Broughton.¹² This sort of physical mechanism and behavior is seen especially in the Si_{60} clusters, as the fullerenelike cage structure shows a pair of multiplets near the Fermi energy in Fig. 5(a) (near -0.5 eV). However, in the case of the Si_{70} cluster, the levels near the Fermi energy are only nearly degenerate, and the gap before and after the distortion is not affected as much. We can also associate the response to the exciton perturbation (discussed in the section below) as related to this level quasidegeneracy near the Fermi level.

Incidentally, one should notice that the HOMO-LUMO gap, as well as the degeneracy of the various levels and Fermi energy of the *ideal* fullerene structures depend strongly on the bond length. For a larger scaling factor (larger bond length), the structures obtained are “metallic” (degenerate or near-degenerate HOMO and LUMO), as mentioned by Khan *et al.* and Menon *et al.*^{12,14} On the other hand, Si_{60} becomes “semiconductor” in our case (Si-Si bond of 2.43 Å). Our choice, moreover, minimizes the total energy of the ideal geometry.

On the other hand, the energy levels for Si_{20} are shown in Figs. 3(c) and 3(d), corresponding to the ideal fullerenelike 3(a) and fully relaxed network structures 3(b), respectively. The ideal fullerenelike structure is “metallic” (for Si-Si bond 2.45 Å) unlike the cases of Si_{60} and Si_{70} representing “semiconductor” behavior. The gap energy for the fully relaxed structure is open to 1.20 eV, however. The different behavior between the small and intermediate silicon clusters would also suggest that the stability of the geometry in the fullerene and network structures is related to the electronic level degeneracy near the Fermi level, as it is split only in the intermediate-size structures.

C. Exciton effects

As described before, we also explore the possibility of light-induced transformations in these small silicon clusters. Since the metastable configurations of the fullerenelike clusters are not the lowest-energy states, one could consider perturbing them by either thermal or other means. To explore the influence of light incident on the structure, we allow for the relaxation of the metastable configuration after the occupation numbers of the system are changed so that an excited electron is promoted to the LUMO. Since this leaves a hole in the HOMO and an electron in the LUMO, it corresponds physically to the absorption of a photon and the creation of an electron-hole exciton pair.

The corresponding resulting structures are shown in Figs. 1(d) and 2(d) for the 60 and 70 cluster. The most obvious

result is that the Si_{60} metastable cage structure is strongly affected by this excitonic perturbation, producing a distortion that approaches the network equilibrium structure in Fig. 1(c). The corresponding electronic spectra is given in Fig. 5(c). Notice that the excitonic perturbation causes a further splitting of the degeneracy for the top filled levels, and forces two orbitals to lie extremely close and on both sides of the Fermi level. The combination of lattice relaxation and electronic level rearrangement in this case *lowers the total energy* (see below).

On the other hand, the excitonic perturbation does not affect appreciably the structure of the Si_{70} cluster, as a comparison between Figs. 2(b) and 2(d) shows. (In fact, only a small change in bond lengths is appreciable there, on the right side of the cluster.) Correspondingly, the change in the level structure [shown in Fig. 6(c)] is not as dramatic either. Although there is an overall spread of the levels near the Fermi level, the corresponding total energy is basically the same in this case, as the electronic rearrangement nearly compensates the small structural one.

To further analyze the structural changes induced by the excitonic perturbation, we also present in Fig. 4 the corresponding pair correlation function for the excited structure (as dashed lines in both panels). Notice that in Si_{70} [Fig. 4(b)] the dashed line is almost identical to the solid line from the metastable structure. Indeed, the exciton produces no appreciable change in the structure. For Si_{60} , however, the dashed line is somewhat in between the metastable and the fully relaxed structure, as an indication of the strong restructuring taking place, which includes overall increased coordination and the creation of a core of atoms inside the cage.

On energetic grounds the picture is also most interesting. For the Si_{70} cluster, the state with the exciton configuration has a higher energy (although only by 0.01 eV/atom, as shown in Table I) than the metastable configuration. This is more like the result one would expect for a static cluster, where only the occupation numbers are allowed to change. On the other hand, for the Si_{60} cluster, the excitonic perturbation induces a wholesale deformation, which is accompanied and/or driven by a *lower* final total energy (by 0.12 eV/atom, see Table I) than the corresponding metastable configuration.

This lowering of the energy and symmetry for Si_{60} clusters can then be seen as a self-trapping of the excitonic excitation (or an “internal conversion” process in photochemistry),²⁸ which would be seen in experiments as a particularly large absorption feature at the corresponding photon energy, and a substantial increase in the lifetime of the associated luminescence (as the exciton would be expected to be longer lived under these circumstances).

One can further intuitively connect the structural changes under the excitonic perturbation and the states involved in the electronic transition. We have calculated the electronic charge density of the orbitals involved, as shown in Fig. 7. The plotted density is calculated from the eigenvectors of the Hamiltonian and represents how the electronic charge is localized around a few atoms on the cluster. This density allows one to understand the mechanism driving the reconstruction of the cluster: Since the photon promotes an electron to the LUMO state, its wave function is changed, creating a nonuniform force field distribution through the

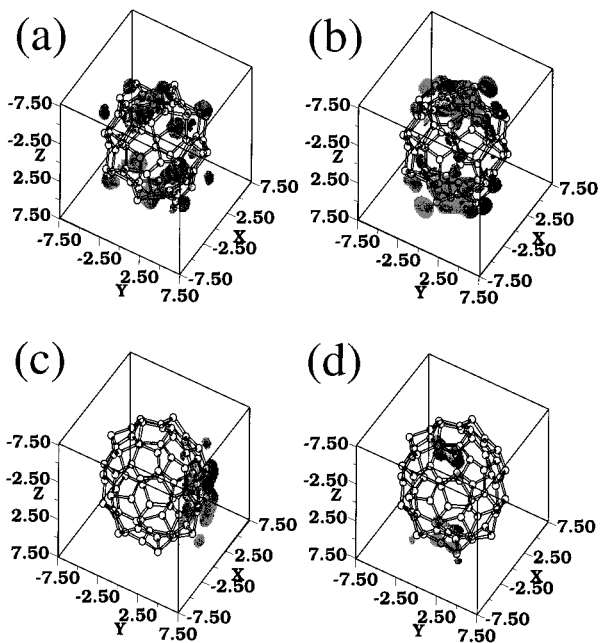


FIG. 7. Charge density for the fullerene-like metastable cage structures. Si_{60} : (a) HOMO and (b) LUMO. Si_{70} : (c) HOMO and (d) LUMO. Notice Si_{70} orbitals are much more localized than in Si_{60} .

cluster, which makes the otherwise (quasi-) equilibrium configuration be unstable (if the force field is strong enough). Correspondingly, Fig. 7 shows the HOMO and LUMO charge densities in a three-dimensional region surrounding the cluster, which should be somewhat related to the force field created by the excitation. Figures 7(a) and 7(b) are for the Si_{60} fullerene-like cage structure HOMO and LUMO, respectively, while Fig. 7(c) and 7(d) for the Si_{70} fullerene-like cage structure. The charge densities in Si_{70} are localized around a few atoms, while those of Si_{60} are more spread over the whole cluster. The details in charge distribution for the different orbitals involved might explain why the effects of an exciton-induced lattice relaxation appear in Si_{60} , and not in Si_{70} . The more complex charge redistribution under photon absorption in the 60 cluster is perhaps more effective in straining many bonds simultaneously, while the more localized charge in Si_{70} does not destabilize the structure.

In order to test further the stability of the fullerene-like cage structure, the system with the exciton perturbation [after full lattice relaxation, as shown in panels (c) in Figs. 1 and 2] is then “relaxed” electronically (the electron in the LUMO is moved back to the HOMO) and then its atoms allowed to relax. The behavior of the structure for this “back relaxation” is very different for the 60 and 70 atom clusters as well. For Si_{70} the structure obtained is basically identical to the fullerene like metastable cage without the exciton [Fig. 2(b)]. This is also evident in the resulting electronic level structure, Fig. 6(d), as it is very close to that of the metastable arrangement in 6(a). In other words, the exciton in Si_{70} is likely a short-lived entity that leaves the structure basically unchanged. This response points to the stability of this metastable state of the 70-atom cluster.

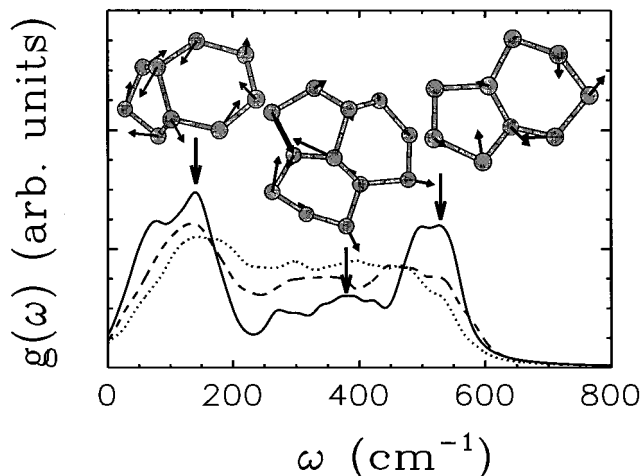


FIG. 8. Vibrational density of states for Si_{60} . Solid, dotted, and dashed lines are fullerene-like cage structure, network structure, and fullerene-like structure with exciton, respectively. Insets show modes at 140, 375, and 527 cm^{-1} .

On the other hand, for the Si_{60} cluster, back relaxation of the self-trapped exciton yields a cluster with energy and bond distribution very close to the fully relaxed cluster in Fig. 1(c). Moreover, the electronic spectrum, as shown in Fig. 5(d), is somewhat close to that of the network structure of Fig. 5(b). This result can be summarized by saying that the equilibrium of the fullerene-like metastable state of the 60 cluster is much more precarious (at least to excitonic perturbations) than the 70 cluster. Once the 60 cluster is perturbed by the photon-induced reconstruction, the fullerene geometry “snaps back” into a more fully relaxed network structure. This complicated response to photoexcitations is reminiscent of the “internal conversion” reaction in photochemistry via a nonradiative process, while in this case the chemistry of the cluster remains unchanged except for internal strains and reconstructions.

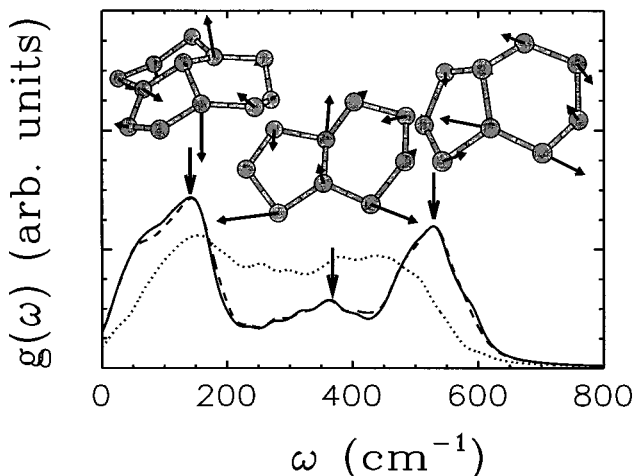


FIG. 9. Vibrational density of states for Si_{70} . Solid, dotted, and dashed lines are fullerene-like cage structure, network structure, and fullerene-like cage structure with exciton, respectively. Insets show modes at 143, 364, and 529 cm^{-1} .

TABLE II. Vibrational modes for Si_{60} and Si_{70} .

| Size | Geometry | Frequency (cm^{-1}) | Mode description |
|------|----------------------------|-----------------------------------|-------------------------------|
| 60 | fullerenelike | 79 | Pentagon and hexagon twisting |
| | | 140 | Pentagon and hexagon twisting |
| | | 273 | Pentagon and hexagon twisting |
| | | | Tetrahedron breathing |
| | | 375 | Two kinds of breathing |
| | | 468 | Tetrahedron breathing |
| | | | Bond stretching |
| | | | Bond stretching |
| 60 | network | 186 | Twisting |
| | | 297 | Twisting |
| | | | Bond stretching |
| | | 462 | Bond stretching |
| 70 | fullerenelike | 143 | Tetrahedron stretching |
| | | 205 | Pentagon and hexagon twisting |
| | | | Bond stretching |
| | | 364 | Tetrahedron breathing |
| 70 | network | 529 | Bond stretching |
| | | 145 | Twisting |
| | | 361 | Twisting |
| | | | Bond stretching |
| 70 | fullerenelike with exciton | 504 | Tetrahedron breathing |
| | | | Bond stretching |
| | | 529 | Pentagon-contract |

As mentioned before, these strong differences between the different size clusters may give rise to substantially different exciton lifetimes, which could be explored by time-resolved spectroscopy of such clusters.

D. Vibrational spectra

The vibrational spectra for silicon clusters of up to seven atoms have been measured by surface plasmon-polariton enhanced Raman spectroscopy and compared successfully to theoretical *ab initio* results.³⁸ However, to our knowledge, little work has been reported on the vibrational spectra of intermediate-size and fullerenelike cage structures.

Figures 8 and 9 show the vibrational spectra for Si_{60} and Si_{70} , respectively. Solid, dotted, and dashed lines are results for the fullerenelike cage structure, the network structure, and the metastable structure with exciton. The spectra obtained from the diagonalization of the dynamical matrix (with 180 and 210 modes in each case, although with few $\omega=0$ modes) are shown as a continuum by using a Lorentzian broadening function with a width of 20 cm^{-1} (which smooths out the distribution but also produces an spurious nonzero value at $\omega=0$). The vibrational density of states then consists of three main broadbands, all below 600 cm^{-1} , and similar to the case of amorphous silicon.³⁹ The first broadband extends to 200 cm^{-1} , while the other two

cover the regions from 200 to 450 cm^{-1} , and from 450 to 600 cm^{-1} in both the 60- and 70-atom clusters.

The identification of the different modes can be made after analyzing the corresponding eigenvectors. The pentagon (and/or hexagon) twisting modes in the structure, where the atoms consisting of pentagons (hexagons) move in phase, are dominant in the region corresponding to the first broadband. The intermediate region is dominated by tetrahedron-breathing modes (much fewer in number in the hollow shell than in the network structures), while the higher-frequency region contains mainly bond-stretching modes. These general trends, however, are a little different for the network structures. The three distinct regions in the fullerenelike structures are much less defined in the network structure, both in nearly equal number of modes throughout the range, and in a slightly reduced range.

In Table II, the main vibrational modes are summarized and described for each structure. For the Si_{60} fullerenelike metastable cage structure, the vibrations at 79 and 140 cm^{-1} are pentagon and hexagon twisting modes, with characteristic eigenvectors as shown in the left inset of Fig. 8 (for the mode at 140 cm^{-1}). Breathing modes appear with the twistings at 273 cm^{-1} . As the mode frequency increases, the twisting modes disappear and the breathing modes become dominant. In particular, at 375 cm^{-1} one has a kind of

breathing mode as shown in the middle inset of Fig. 8, moving inward and outward from the shell. Moreover, bond stretching and compressing modes exist at about 468 cm^{-1} . Finally, for 500 and 527 cm^{-1} , the structure is dominated by the bond-stretching modes as shown in the right inset of Fig. 8 (for the mode at 527 cm^{-1}). Notice, on the other hand, that the network structure of the 60-atom cluster has strong mixing of twisting and bond-stretching modes, making a unique classification much more difficult.

For the Si_{70} fullerene-like cage structure, the general trends of the main broadbands are the same as for Si_{60} , except for the tetrahedron stretching modes. These latter modes are dominant at the vibrational frequency 143 cm^{-1} , and shown in the left inset of Fig. 9. The modes illustrate the vectors for the pentagon (hexagon) twisting, breathing at 364 cm^{-1} (shown in the middle inset of Fig. 9), and bond-stretching modes at 529 cm^{-1} (shown in the right inset of Fig. 9), corresponding to each band. On the other hand, the interesting pentagon-contract modes for the Si_{70} fullerene-like structure with exciton is shown.

IV. CONCLUSIONS

We have studied the geometrical structures and the electronic and vibrational spectra of fullerene-like cage and network structures in intermediate-size silicon clusters with 20, 60, and 70 atoms. A first-principles quantum molecular-dynamics method developed by Sankey and co-workers is used. As expected for larger clusters, we find that the lowest-energy configuration is typically a network structure with a high degree of coordination for atoms in the inner core of the cluster, saturating dangling bonds introduced by the finite size of the structure. However, we also find fullerene-like cage structures in Si_{60} and Si_{70} are metastable, with a mod-

erate degree of stability, and show a similar coordination to the ideal fullerene structure but made out of silicon. The equilibrium network structures are more energetically stable than the fullerene-like cage structures by typically 0.25 eV/atom .

By studying the relaxation process of these clusters, we find that it takes place (or is driven by) an interesting breaking of the symmetry and accompanied by splitting of degenerate or near-degenerate states near the Fermi level. This behavior is reminiscent of the Jahn-Teller distortions in solids, where the restructuring energetics is compensated by the shift in the electronic level structure.

Very interesting as well, we have studied the effects of an exciton-induced lattice relaxation in these systems. The lattice distortion associated with exciton leads to a splitting of the degeneracy, and results in lower energy and lower symmetry. Most interestingly, the Si_{60} structure is much more strongly affected by the formation of an exciton (by photon absorption) than the corresponding 70-atom cluster. The relaxation that ensues after the photon absorption and the overall reduction of the energy of the system imply that the exciton is self-trapped. This in turn would produce a longer lifetime of the exciton, which could be possibly monitored in time-resolved photoluminescence measurements. We hope this work would motivate such experiments.

ACKNOWLEDGMENTS

We would like to thank D.R. Alfonso, R.L. Cappelletti, M. Cobb, and M. Menon for helpful discussions and comments. This work was partially supported by the U.S. Department of Energy through Grant No. DE-FG02-91ER45334 and NSF Grant No. DMR-93-22412, as well as by the A. von Humboldt Foundation (S.E.U.).

-
- ¹D. Tománek and M. A. Schlüter, *Phys. Rev. B* **36**, 1208 (1987).
²O. F. Sankey, D. J. Niklewski, D. A. Drabold, and J. D. Dow, *Phys. Rev. B* **41**, 12 750 (1990).
³M. F. Jarrold and V. A. Constant, *Phys. Rev. Lett.* **67**, 2994 (1991); M. F. Jarrold and J. E. Bower, *J. Chem. Phys.* **96**, 9180 (1992); M. F. Jarrold, *Science* **252**, 1085 (1991).
⁴K. Raghavachari, *J. Chem. Phys.* **84**, 5672 (1986).
⁵K. Raghavachari and C. M. Rohlfing, *J. Chem. Phys.* **89**, 2219 (1988).
⁶L. A. Bloomfield, R. R. Freeman, and W. L. Brown, *Phys. Rev. Lett.* **54**, 2246 (1985).
⁷J. L. Elkind, J. M. Alford, F. D. Weiss, R. T. Laaksonen, and R. E. Smalley, *J. Chem. Phys.* **87**, 2397 (1987).
⁸J. R. Chelikowsky and J. C. Phillips, *Phys. Rev. Lett.* **63**, 1653 (1989).
⁹K. Fuke, K. Tsukamoto, F. Misaizu, and M. Sanekata, *J. Chem. Phys.* **99**, 7807 (1993).
¹⁰K. D. Rinnen and M. L. Mandich, *Phys. Rev. Lett.* **69**, 1823 (1992).
¹¹P. Ordejón, D. Lebedenko, and M. Menon, *Phys. Rev. B* **50**, 5645 (1994).
¹²F. S. Khan and J. Q. Broughton, *Phys. Rev. B* **43**, 11 754 (1991).
¹³M. C. Piqueras, R. Crespo, E. Ortí, and F. Tomás, *Chem. Phys. Lett.* **213**, 509 (1993).
¹⁴M. Menon and K. R. Subbaswamy, *Chem. Phys. Lett.* **219**, 219 (1994).
¹⁵J. R. Chelikowsky and J. C. Phillips, *Phys. Rev. B* **41**, 5735 (1990); J. R. Chelikowsky, K. M. Glassford, and J. C. Phillips, *ibid.* **44**, 1538 (1991).
¹⁶K. Kobayashi and S. Nagase, *Bull. Chem. Soc. Jpn.* **66**, 3334 (1993).
¹⁷E. Kaxiras and K. Jackson, *Phys. Rev. Lett.* **71**, 727 (1993).
¹⁸U. Röthlisberger, W. Andreoni, and M. Parrinello, *Phys. Rev. Lett.* **72**, 665 (1994).
¹⁹E. Kaxiras, *Phys. Rev. Lett.* **64**, 551 (1990).
²⁰M. Menon and K. R. Subbaswamy, *Phys. Rev. B* **47**, 12 754 (1993).
²¹M. Menon and K. R. Subbaswamy, *Phys. Rev. B* **51**, 17 952 (1995).
²²J. C. Grossman and L. Mitás, *Phys. Rev. Lett.* **74**, 1323 (1995).
²³See, for example, *Solid State Physics* (Academic, Boston, 1994), Vol. 48, Chap. I.
²⁴O. Pankratov and M. Scheffler, *Phys. Rev. Lett.* **71**, 2797 (1993).
²⁵G. B. Adams, O. F. Sankey, J. B. Page, and M. O'Keeffe, *Chem. Phys.* **176**, 61 (1993).
²⁶F. Mauri and R. Car, *Phys. Rev. Lett.* **75**, 3166 (1995).
²⁷P. A. Fedders, Y. Fu, and D. A. Drabold, *Phys. Rev. Lett.* **68**, 1888 (1992).

- ²⁸I. N. Levine, *Physical Chemistry* (McGraw-Hill, New York, 1988).
- ²⁹O. F. Sankey and D. J. Niklewski, *Phys. Rev. B* **40**, 3979 (1989); O. F. Sankey, D. A. Drabold, and G. B. Adams, *Bull. Am. Phys. Soc.* **36**, 924 (1991).
- ³⁰J. Harris, *Phys. Rev. B* **31**, 1770 (1985).
- ³¹W. Kohn and L. J. Sham, *Phys. Rev.* **140**, A1133 (1965).
- ³²D. M. Ceperley and G. J. Adler, *Phys. Rev. Lett.* **45**, 566 (1980); J. Perdew and A. Zunger, *Phys. Rev. B* **23**, 5048 (1981).
- ³³D. R. Hamann, M. Schlüter, and C. Chiang, *Phys. Rev. Lett.* **43**, 1494 (1979).
- ³⁴D. E. Milligan and M. E. Jacox, *J. Chem. Phys.* **52**, 2594 (1970).
- ³⁵G. B. Adams *et al.*, *Science* **256**, 1792 (1992); D. A. Drabold *et al.*, *Phys. Rev. B* **49**, 16 415 (1994); D. A. Alfonso *et al.*, *ibid.* **51**, 14 669 (1995).
- ³⁶K. A. Jackson and M. R. Pederson, *Phys. Rev. Lett.* **67**, 2521(1991).
- ³⁷M. S. Hybertsen and S. G. Louie, *Phys. Rev. B* **34**, 5390 (1986).
- ³⁸E. C. Honea, A. Ogura, C. A. Murray, K. Raghavachari, W. O. Sprenger, M. F. Jarrold, and W. L. Brown, *Nature* **366**, 42 (1993).
- ³⁹P. A. Fedders, D. A. Drabold, and S. Klemm, *Phys. Rev. B* **45**, 4048 (1992).